NASA TECHNICAL MEMORANDUM

NASA TM X-68047

NASA TM X-68047

PEAK AXIAL-VELOCITY DECAY WITH MULTI-ELEMENT RECTANGULAR AND TRIANGULAR NOZZLES

by D. E. Groesbeck, U. H. von Glahn
and R. G. Huff
Lewis Research Center
Cleveland, Ohio

March, 1972

This information is being published in preliminary form in order to expedite its early release.

PEAK AXIAL-VELOCITY DECAY WITH MULTI-ELEMENT RECTANGULAR AND TRIANGULAR NOZZLES

by

D. E. Groesbeck, U. H. von Glahn
and R. G. Huff

INTRODUCTION

Of the several lift augmentation concepts proposed for STOL aircraft, the present study is concerned with externally blown flaps (fig. 1). Experimental studies have shown that the impingement of the engine exhaust jet on deflected flaps can cause an unacceptable increase in the aircraft noise signature. The jet-flap interaction noise can be lowered by reducing the impinging velocity on the flap. This velocity reduction generally must be accomplished in a specified distance from the jet exhaust plane to the flap.

The jet velocity impinging on the flap can be reduced by: (1) a reduction of the jet velocity at the exhaust by utilizing large bypass-type fan engines and (2) by use of a mixer-type nozzle, consisting of multi-elements rather than a single large exhaust nozzle of equal total area. The individual small elements of a mixer nozzle promote an initially rapid mixing with the surrounding air resulting in a rapid axial velocity decay.

This paper summarizes the results of an experimental study conducted at the NASA Lewis Research Center, on the peak axial-velocity decay obtained with rectangular and triangular single-element and multi-element mixer nozzles. Empirical equations are developed for estimating peak axial-velocity decay curves for a wide range of nozzle configurations.

APPARATUS AND PROCEDURE

Test stand. - The test stand used in the present work is shown in figure 2. Pressurized air at about 289 K is supplied to a 15.25-cm diameter plenum by twin diametrically opposed supply lines. Flexible couplings in each of the twin supply lines isolate the supply system from a force measuring system. The plenum is free to move axially through an overhead cable suspension system. A load cell at the upstream end of the plenum is used to measure thrust. The test nozzles were attached to a flange at the downstream end of the plenum.

Airflow through the overhead main supply line was measured with a calibrated orifice. The nominal nozzle inlet total pressure was measured with a single probe near the plenum exit flange.

A traversing probe was first positioned 0.317-cm from the nozzle exit plane and radial pressure-traverses were made in the plane of the pertinent element dimension (i.e., length of a triangular element, width of a rectangular element, etc.). Pressure measurements were obtained at nominal nozzle pressure ratios of 1.15, 1.3, 1.53, 1.87, and 2.3. This procedure was then repeated at nominal distances from the nozzle exit plane of 13-, 25-, 38- and 51-cm. Initially in the program a single pitot-static probe was moved manually to various locations from 100- to 300-cm downstream of the nozzle exit plane and pressure data recorded. Near the end of the program the traversing probe track was extended to cover the full range of axial distances.

The measurements from the traversing probe were transmitted to an x-y-y' plotter which yielded direct traces on graph paper of the total and static

pressure distribution radially across the jet. All other pressure data were recorded from multitube water or mercury manometers.

CONFIGURATIONS

Peak axial velocity decay data were obtained with single-element triangular and rectangular nozzles. The studies included variations in nozzle aspect ratio and nozzle area.

The rectangular multi-element nozzles tested included 3 and 6 slot configurations. The spacing between elements was varied to evaluate its effect on peak axial-velocity decay. Typical multi-element nozzles are shown in figure 3. Pertinent dimensions for the nozzles tested are summarized in Table I.

RESULTS AND DISCUSSION

GENERAL

According to the literature (refs. 1 and 2), the peak axial velocity decay downstream of the jet core varies as a function of X^{-1} for circular nozzles to $X^{-\frac{1}{2}}$ for infinite or large aspect ratio rectangular (slot) nozzles. (All symbols are defined in the appendix.) For other single-element geometries the decay appears to vary between these exponents. The axial distance is nondimensionlized by the effective diameter of the element; i.e., X/D_e.

For multi-element nozzles, the initial peak axial-velocity decay (fig. 4), is substantially the same as that for an individual element. However, at some distance downstream of the nozzle exit plane, the individual jets coalesce sufficiently to form a large diameter coalescing core and

a very slow peak-velocity decay occurs. Once the coalesced core has fully formed, normal mixing again occurs with an associated rapid velocity decay. It was determined previously (ref. 3) that the axial decay distance for multi-element nozzles could be nondimensionalized for correlation purposes by the use of an effective diameter based on that of a single element.

The peak velocity ratio at a given axial station has been found to increase with increasing jet Mach number (refs. 3 to 6). Correlation of the jet Mach number for both single- and multi-element nozzles was achieved in references 3 and 6 by dividing the axial distance parameter, X/D_e, by $\sqrt{1+M_j}$. In order to avoid confusing the figures herein with a large number of data points, only the nominal 0.99 jet Mach number data, unless specifically noted, will be shown.

The following sections will present decay data for a variety of single-element nozzles and multi-element configurations together with correlating equations.

CORRELATION

Reference 6 presents empirical equations for predicting the peak axial-velocity decay for single- and multi-element nozzles. The equations are repeated herein for convenience and where necessary extended to fit more closely the data obtained with large aspect-ratio rectangular nozzles.

Single-Element Nozzles

The peak axial-velocity decay was correlated in reference 6 by the following equations:

$$\frac{U}{U_j} = \left[1 + \left(\frac{0.15\ X}{C_n\ D_e\sqrt{1+M_j}}\right)^a\right]^{-1/a} \tag{1}$$

where

$$a = 4(2 - h_i/h_o)\left(1 + 2.67((D_e/D_h) - 1)\right)^{-1} \qquad (2)$$

Examination of single-element nozzle data showed that these simple empirical equations generally provided good correlation. With increasing aspect ratio for rectangular nozzles, however, the equations predicted increasingly optimistic velocity decay values with axial distances downstream of the nozzle exit plane.

It was determined from data cross-plots that an extension of equation (2) could provide a better fit between the empirical predictions and the experimental data. Thus, the exponent a (eq. (2)) should be replaced by a' as follows:

$$a' = a\left[1 + \left\{\frac{2.67}{(1 + 0.0001\ (L/h)^3)\left(\frac{X}{C_n\ D_e\sqrt{1+M_j}}\right)}\right\}^3\right] \qquad (3)$$

Rewriting equation (1) with the exponent given by equation (3) results in the following extended correlation relationship:

$$\frac{U}{U_j} = \left[1 + \left(\frac{0.15\ X}{C_n\ D_e\sqrt{1+M_j}}\right)^{a'}\right]^{-\frac{1}{a'}} \qquad (4)$$

Calculated decay curves using equations (3) and (4) are shown in figure 5 for three rectangular nozzles with (L/h) values of 1.5, 12 and 24, respectively, together with the experimental data. Also shown are curves based on equations (1) and (2). The better fit of the curve based on equations (3) and (4) is apparent, particularly for larger L/h values, such at the reference 2 data, where L/h is 24.

Multi-Element Nozzles

In reference 6 empirical equations also were developed to correlate the peak axial-velocity decay of multi-element nozzles in terms of the significant flow regimes shown previously in figure 4 and in terms of pertinent nozzle dimension parameters. These equations are limited, in general, by the nozzle geometries tested; however, they are useful in predicting the decay curves for many practical nozzle configurations.

The decay curve was divided into several regions shown in figure 6. Equations were then developed to predict the departure point of the coalescing core from the single-element decay curve (point (1)). Examination of the data showed that the velocity ratio in the coalescing core decay region had a slope of -0.2 with respect to axial distance (region denoted by (1) to (2)). The nondimensional displacement parameter, D_x, of the coalesced-core decay curve from the single-element curve was then determined. The value of U/U_j at point (2) was then correlated in terms of the coalescing core decay slope and the displacement distance D_x. Finally, the correlation equation for the decay curve of the fully coalesced core was established.

Empirical equations for the preceding points and regions are given in the following paragraphs.

The departure point (1) is calculated by the following general equation:

$$\left(\frac{X}{C_n D_e \sqrt{1 + M_j}}\right)_{(1)} = Z_{(1)} = 12\left(1 + \frac{1}{4}\left(\frac{s}{w}\right)^{2/3}\right)\left(\frac{s}{w}\right)^{1/3} f\left(\frac{D_e}{D_h}\right) f\left(\frac{r}{s}\right) \qquad (5)$$

where $w = h$ for the present configurations.

The functions in equation (5) are given by:

$$f\left(\frac{D_e}{D_h}\right) = \left[1 + \frac{2.67\left(\frac{D_e}{D_h} - 1\right)}{1 + 5\left(1 - \frac{h_i}{h_o}\right)^8}\right]^{-1} \tag{6}$$

for the present configurations, and

$$f\left(\frac{r}{s}\right) = \left[1 + 0.33\,\frac{r}{s}\,(f(w))^3\left(\frac{U_s}{U_c}\right)^2\right]^{-1} \tag{7}$$

in which $r = s_H$ and $(f(w))^3 = 1$ (see also ref. 6) for the present configurations. The data for multi-element nozzles with large aspect ratios suggest that equation (5) is a function of (L/h). Good correlation can be achieved by dividing equation (5) by the following aspect ratio relation:

$$\left[1 + 0.0025\left(\frac{L}{h} - 1\right)^2\right] \tag{8}$$

where L and h values for various configurations are given in Table I.

The displacement of the fully coalesced multi-element core from the single element curve (D_x in fig. 6), in general, is calculated from the following equation:

$$D_x = 1 + \left(\sqrt{\frac{A_c + A_s\left(\frac{U_s}{U_c}\right)^2}{A_e}} - 1\right)\left[1 + \frac{s}{w}\left(\frac{1}{1 + 50\left(\frac{D_e}{D_h} - 1\right)^{5/3}}\right)\right]^{-1/2} \tag{9}$$

When U_s/U_c equals 1, the term $\sqrt{\frac{A_c + A_s\left(\frac{U_s}{U_c}\right)^2}{A_e}}$ in equation (9) reduces to $\frac{D_{e,T}}{D_e}$.

The velocity decay in the coalescing core (region ① to ②) is given by the following relationship:

$$\left|\frac{U}{U_j}\right|_{① \to ②} = \left|\left(\frac{U}{U_j}\right)_{①}\left(\frac{\frac{Z_{①}}{X}}{C_n D_e \sqrt{1 + M_j}}\right)^{1/5}\right|_{① \to ②} \tag{10}$$

In the coalesced core region (fig. 6) the velocity ratio is given by:

$$\left|\frac{U}{U_j}\right|_{② \to \infty} = \left|\left[1 + \left(\frac{0.15\ X}{D_x C_n D_e \sqrt{1 + M_j}}\right)^{a'}\right]^{-1/a'}\right|_{② \to \infty} \tag{11}$$

The intersection of curves calculated from equations (9) and (10) provides the location of point ② in figure 6.

EXPERIMENTAL DATA

Single-Element Nozzles

The peak axial-velocity decay for four single-element, sharp-edged rectangular-orifice nozzles with nominal L/h values varying from 2.22 to 11.25 are shown in figure 7. These configurations were studied, in addition to those of reference 6, to help in establishing trends due to geometry variations. In all cases, the normalizing coefficient, C_n, was 0.67 (as also in the cases given in ref. 6). The curves shown in figure 7 were

calculated using equations (3) and (4). The data indicate that with increasing L/h values, the initial velocity decays more rapidly. As jet mixing proceeds farther downstream from the nozzle exit plane, the velocity decay for all nozzles becomes substantially the same.

The peak axial-velocity decay obtained with four rectangular convergent nozzles is shown in figure 8. The circle symbols are data for a single element of the present rectangular nozzle (fig. 3(a)) while the square and diamond symbols are data for single elements of the 6-slot nozzle shown in figure 3(b). Velocity decay data for the 2.75 by 16.55 cm rectangular nozzle taken from reference 5 are shown in figure 8(b). The data trends are similar to those noted for the orifice-type nozzles (fig. 7) and are well correlated by equations (3) and (4).

Triangular nozzles. - The peak axial-velocity decay data together with calculated curves are shown in figure 9. The velocity decay trends are similar to those noted for rectangular nozzles. These data are also shown in reference 3 and are included herein for comparison with calculated values obtained with the equations (3) and (4).

Multi-Element Nozzles

Rectangular nozzles. - Peak velocity decay data for the present 3-slot rectangular nozzle (fig. 3(a)) are shown in figure 10 together with calculated curves. The data are for spacings between the nozzle elements of 4.32 and 6.35 cm. As in all previously tested nozzles, increasing the spacing ratio caused the departure point of the coalescing core from the single-element curve to occur at a large downstream axial distance. This was also accompanied by a decrease in U/U_j at the departure points.

The 4-slot rectangular nozzle (ref. 5) is shown in figure 11 together with the calculated curve. The data are similar to that for the 3-slot rectangular nozzle and are well represented by the correlation equations.

The modifications to the reference 6 correlation equations in order to obtain a better fit to the data can be considered as a need by large aspect ratio multi-element rectangular nozzles for additional ventilation, compared with multitube and multi-lobe nozzles, to promote mixing with the surrounding ambient air. This was first noted when multi-element rectangular-orifice nozzles were tested. The velocity surveys near the nozzle exhaust plane for these configurations showed significant sub-atmospheric pressure near the base between the adjacent jets issuing from the orifices. As a consequence, the velocity decay was adversely affected over the entire range of conditions sutided and the data are not included herein. Thus, it appears that well-ventilated multi-orifice configurations (multi-hole, multi-lobe, etc.) can be used successfully in velocity decay screening tests; however the use of orifices should be avoided for multiple rectangular slots.

The 4-slot nozzle of reference 5 was also tested with divergent walls (narrow side), in which the divergent wall angle, β, for each side was varied to 5, 15 and 30°. These data were obtained with a spacing ratio (as defined herein) of 2.0. In plotting the data from reference 5 using the present parameters, an effect of β was apparent. The data spread with divergent wall angle could be correlated by including a β -parameter in the distance parameter as follows:

$$\frac{X\,(1 + \sin^2\beta)}{C_n D_e \sqrt{1 + M_j}} \qquad (12)$$

The correlated velocity decay data using equation (12) is shown in figure 12. Also shown is the calculated curve in which the term $(1 + \sin^2\beta)$ has now been included as a multiplier wherever $\frac{X}{C_n D_e \sqrt{1 + M_j}}$ is used in the empirical equations.

The effect of spacing ratio with the 4-slot nozzle data of reference 5 is shown in figure 13 for a nozzle with a β value of 15°. As shown good correlation between calculated and experimental values is obtained except with a spacing ratio of 0.5.

The effect of changes in nozzle L/h values from 3 to 10 are shown in figure 14 for the 4-slot nozzle of reference 5. Again, the β value was 15°. The calculated curves show a good agreement with the experimental data as would be expected from the previous data presentation.

Ventilated (split-element) slot nozzles. - In an effort to study the effect of additional ventilation on the velocity decay of multi-element rectangular nozzles, centerbodies of 3.81 and 6.35 cm, respectively, were inserted in the middle of each element of the 3-slot nozzle having an element spacing of 6.35 cm (fig. 3(b)). The centerbodies provided a spacing ratio s_H/L, of 0.46 and 0.91, respectively. Thereby, additional ventilation entries for the surrounding ambient air was provided at the centerbody locations.

Peak axial-velocity decay curves for the split-element nozzles are shown in figure 15. The decay data were obtained at the centerline of the left half of the split-element nozzles for the first 50 cm, shown by the clear symbols, and also at the overall nozzle centerlines, shown by the tailed symbols. The data taken at the nozzle centerline show that a gradual mixing

occurs with increasing distance downstream of the nozzle and the velocity ratio U/U_j is much less than that at the element centerline. It is only in the coalesced-core regime that the velocity ratio at the nozzle centerline becomes the dominant peak value.

It is to be expected that as the centerbody of the split-element nozzles is decreased in size (decreasing s_H) while maintaining the s/h, an interaction of the adjacent jets will occur that will influence the velocity decay. For very small values of s_H, the jets should coalesce quickly to a single large aspect ratio rectangular jet and decay more like those shown in figure 10. An empirical equation for this type of jet coalescence is presently not available.

Triangular lobed nozzle. - In reference 5 the velocity decay of a 12-lobe triangular-element nozzle is reported. The data were also shown in reference 3. These peak axial-velocity decay data are repeated herein and compared with calculated curves in figure 16. In general, good agreement exists between the calculated and measured values. In the region of single-element decay, the modified equations presented herein provide excellent agreement while the departure point is also predicted.

CONCLUDING REMARKS

Jet axial-velocity decay data are reported for single element and multi-element rectangular and triangular nozzles for application to externally-blown-flap STOL aircraft. These data extend knowledge toward a rational design approach to nozzles that mix rapidly with the surrounding air for the purpose of reducing the noise caused by the interaction of jet

impingement on the flap assembly. The empirical relationships that are presented permit, for the most part, the prediction of peak axial-velocity decay curves. However, they are not sufficiently general to permit their use when the spacing ratio approaches zero. With close element-spacings and/or multi-directional spacings, a multiplicity of decay curves can be expected as first one spacing ratio and then another influence the velocity decay. Also equation (7) becomes invalid when $s = 0$. Consequently, additional experimental work and data correlation remains to be accomplished in the general field of jet velocity decay for specific applications.

Use of a mixer nozzle for reducing the jet-flap interaction noise from an externally blown flap in STOL aircraft applications must consider not only the effect of the reduction of the impinging velocity on the flap, but also the increased jet impingement area on the flap as well as impingement along the wing surface. This increased area is caused by the larger overall dimensions of the mixer-nozzle jet compared with that for a conventional circular-nozzle jet. Thus, the full jet-flap interaction noise benefits resulting from the velocity decay associated with a mixer nozzle may be significantly reduced by the larger jet impingement area.

SYMBOLS

A_c	area of core nozzle, cm^2
A_e	area of single element, cm^2
A_s	area of bypass nozzle, cm^2
h, L, r, s, s_H, w	nozzle dimensions, cm (see also Table I)
C_n	effective nozzle (or orifice) coefficient
D_e	effective diameter of circular nozzle with exit area equal to that of noncircular single element (D_e for a circular nozzle equals the nozzle diameter), cm
$D_{e,T}$	effective diameter of circular nozzle with exit area equal to that of total multi-element nozzle area, cm
D_h	hydraulic diameter of nozzle element, cm
D_x	analytical displacement parameter
M_j	jet Mach number
$s/w, r/w$	ratio of effective spacing between adjacent jets (including nozzle wall thickness) at nozzle exit plane to effective element width
U	local peak axial-velocity of jet, m/sec
U_j	jet exhaust velocity, m/sec
U_s/U_c	ratio of bypass jet velocity to core jet velocity
X	axial distance downstream of effective nozzle exit plane, cm
$Z_{(1)}$	defined by equation (5)
β	wall divergence angle, deg.

Subscripts:

i	effective minimum
n	nozzle
o	effective maximum

REFERENCES

1. Landis, Fred; and Shapiro, Ascher H.: The Turbulent Mixing of Co-Axial Gas Jets. Proceedings of Heat Transfer and Fluid Mechanics Institute. Stanford University Press, 1951, pp. 133-146.

2. Weinstein, A. S.; Osterle, J. F.; and Forstall, W.: Momentum Diffusion From a Slot Jet Into a Moving Secondary. J. Appl. Mech., vol. 23, no. 3, Sept. 1956, pp. 437-443.

3. Groesbeck, D.; Huff, R.; and von Glahn, U.: Peak Axial-Velocity Decay with Mixer-Type Exhaust Nozzles. NASA TM X-67934, 1971.

4. Higgins, C. C.; and Wainwright, T. W.: Dynamic Pressure and Thrust Characteristics of Cold Jets Discharging from Several Exhaust Nozzles Designed for VTOL Downwash Suppression. NASA TN D-2263, 1964.

5. Higgins, C. C ; Kelley, D. P.; and Wainwright, T. W.: Exhaust Jet Wake and Thrust Characteristics of Several Nozzles Designed for VTOL Downwash Suppression. Tests in and Out of Ground Effect with 70° F and 1200° F Nozzle Discharge Temperatures. NASA CR-373, 1966.

6. von Glahn, U. H.; Groesbeck, D. E.; and Huff, R. G.: Peak Axial-Velocity Decay with Single- and Multi-Element Nozzles. Paper 72-48, AIAA, Jan. 1972.

TABLE I NOMINAL NOZZLE DIMENSIONS

Single-Element Nozzles

Rectangular

Height, h, cm	Length, L, cm	Nominal Aspect Ratio	Type	Reference
1.27	15.25	12	orifice	3,6
2.54	15.25	6		
5.08	15.25	3		
5.08	7.62	1.5		
1.02	11.42	11.2		present
1.52	11.42	7.5		
2.29	5.08	2.2		
2.29	11.42	5		
1.52	20.32	13.3	nozzle	
2.75	16.55	6		4,5
1.52	8.25	5.4		present
1.52	7.0	4.6		

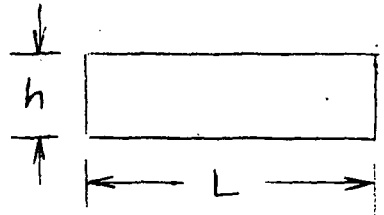

Triangular

2.54	15.25		orifice	3
5.08	15.25			
5.08	7.62			

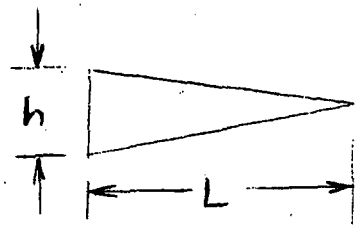

TABLE I · NOMINAL NOZZLE DIMENSIONS (con't)

ulti-Element Nozzles

ectangular

	Height, h, cm	Length, L, cm	s, cm	s_H, cm	β, deg.	Nominal Aspect Ratio	Reference
3-slot	1.52	20.32	6.35	--	0	13.3	present
↓	1.52	20.32	4.32	--	0	13.3	↓
4-slot	1.51	7.55	2.27	--	15	5.0	5
			3.02	--	15	5.0	
			4.53	--	0,5,15,30	5.0	
			6.05	--	15	5.0	
	1.95	5.83	5.83	--	15	3.0	
	1.07	10.68	3.20	--	15	10.0	
6-slot	1.52	8.25	6.35	3.81	0	5.4	present
↓	1.52	7.0	6.35	6.35	0	4.6	↓

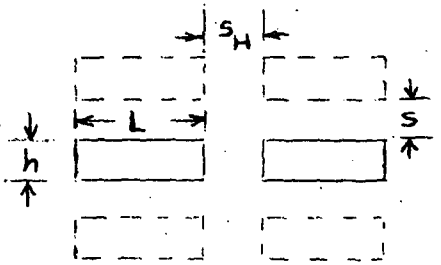

Triangular

			s/h				
12-lobe	0.76	8.4	4	--	--		4,5

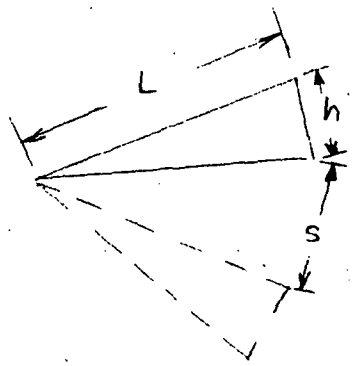

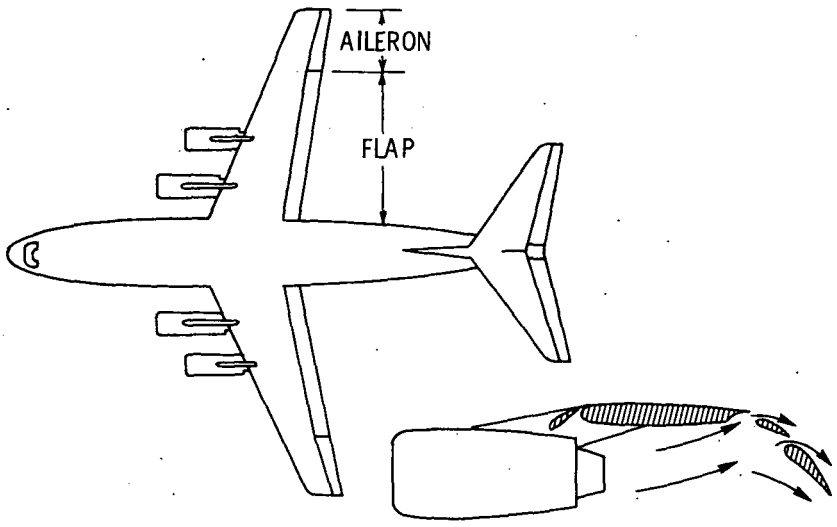

Figure 1. - Externally-blown-flap STOL airplane.

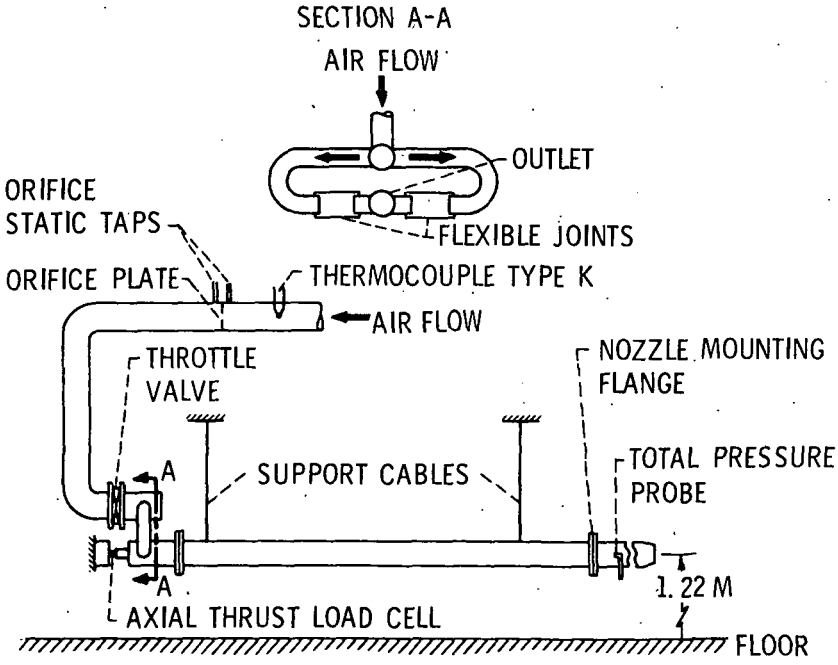

Figure 2. - Schematic diagram of test rig.

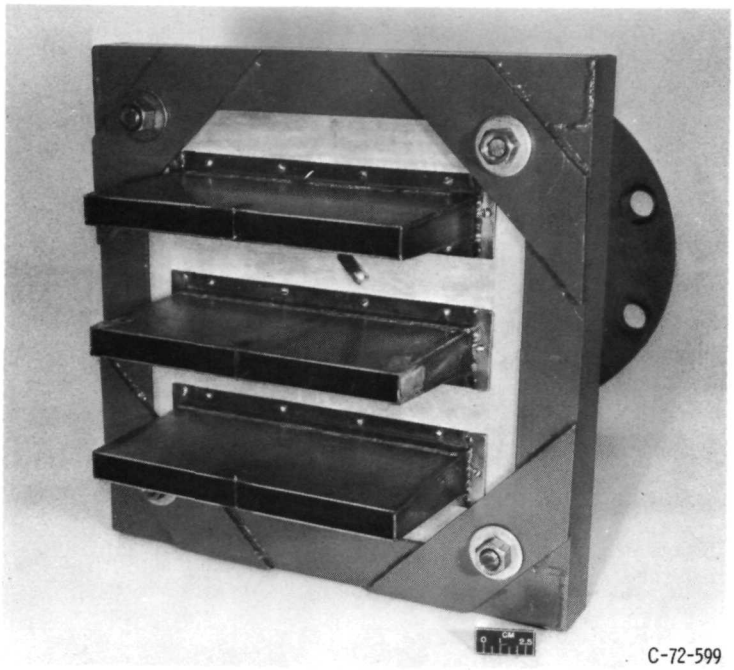

C-72-599

(a) 3-slot rectangular nozzle.

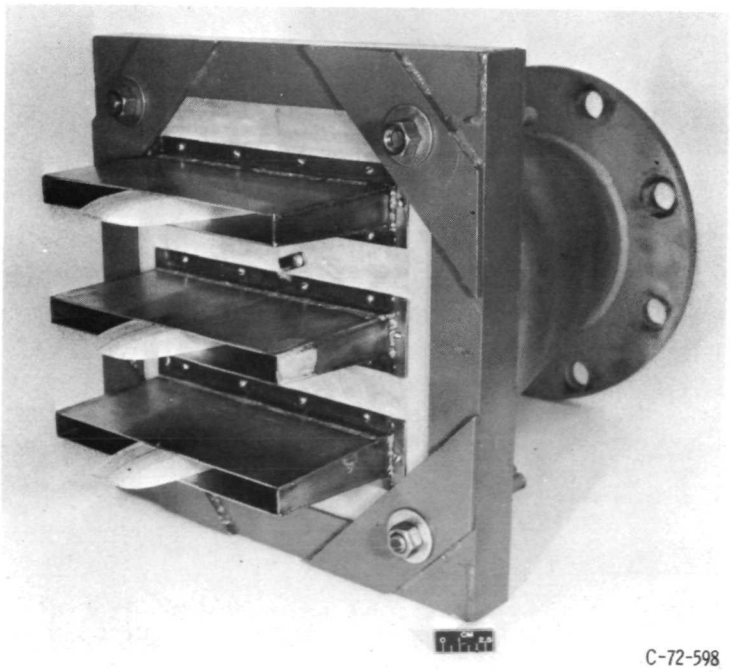

C-72-598

(b) 6-slot split-element nozzle.

Figure 3. - Typical rectangular multi-element nozzles.

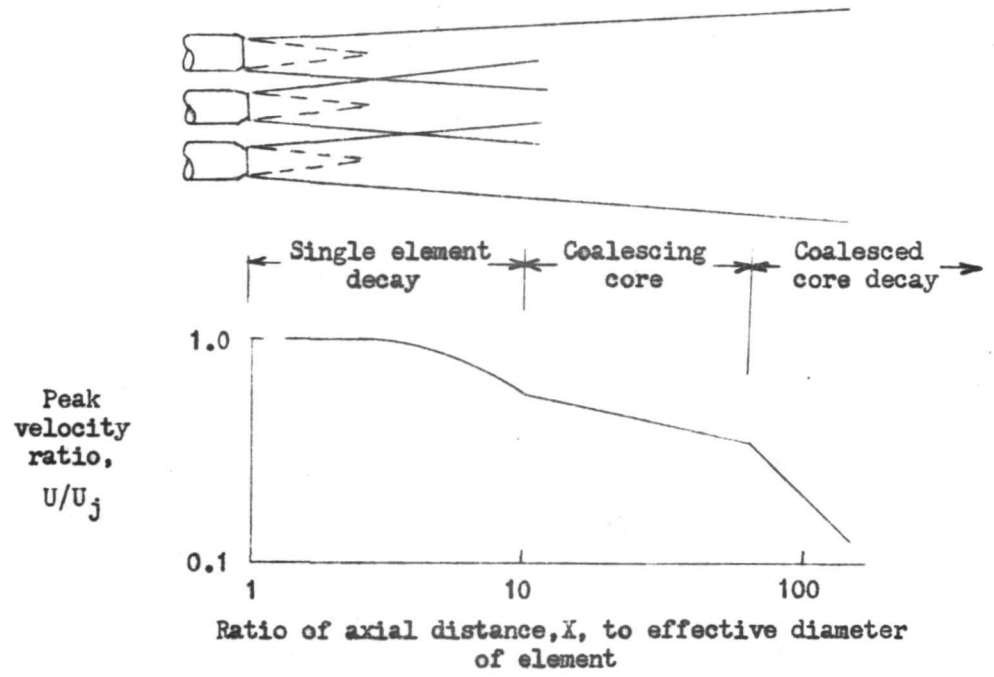

Figure 4. - Schematic of multi-element nozzle peak axial-velocity decay.

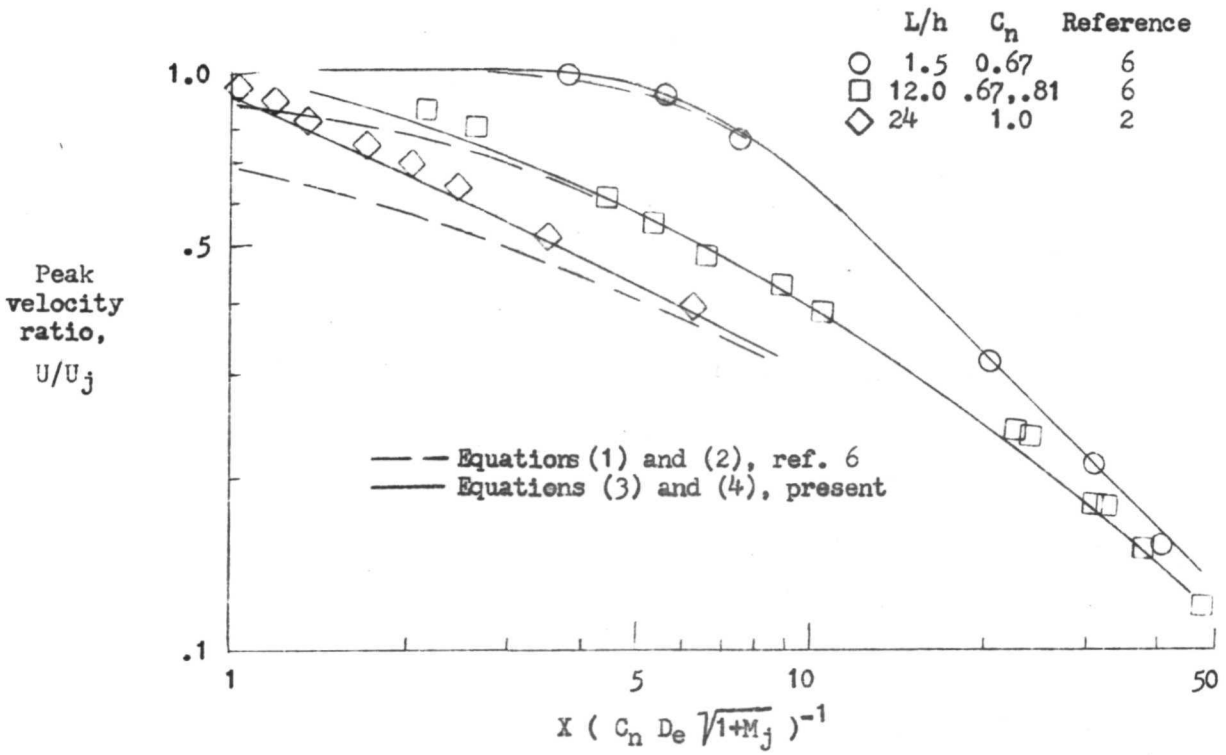

Figure 5. - Comparison of calculated decay curves with data for several rectangular-orifice nozzles with various aspect ratios.

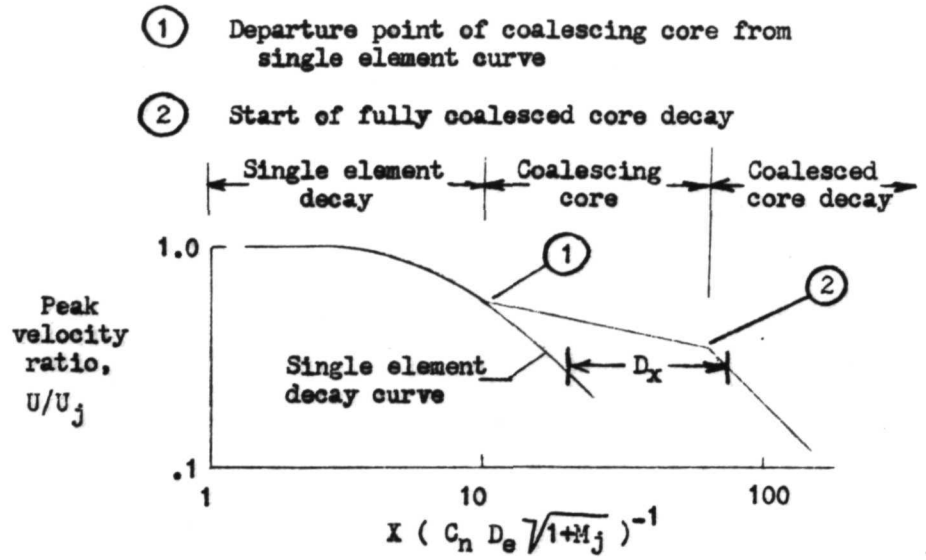

Figure 6. - Significant mixed-flow regimes for multi-element nozzles.

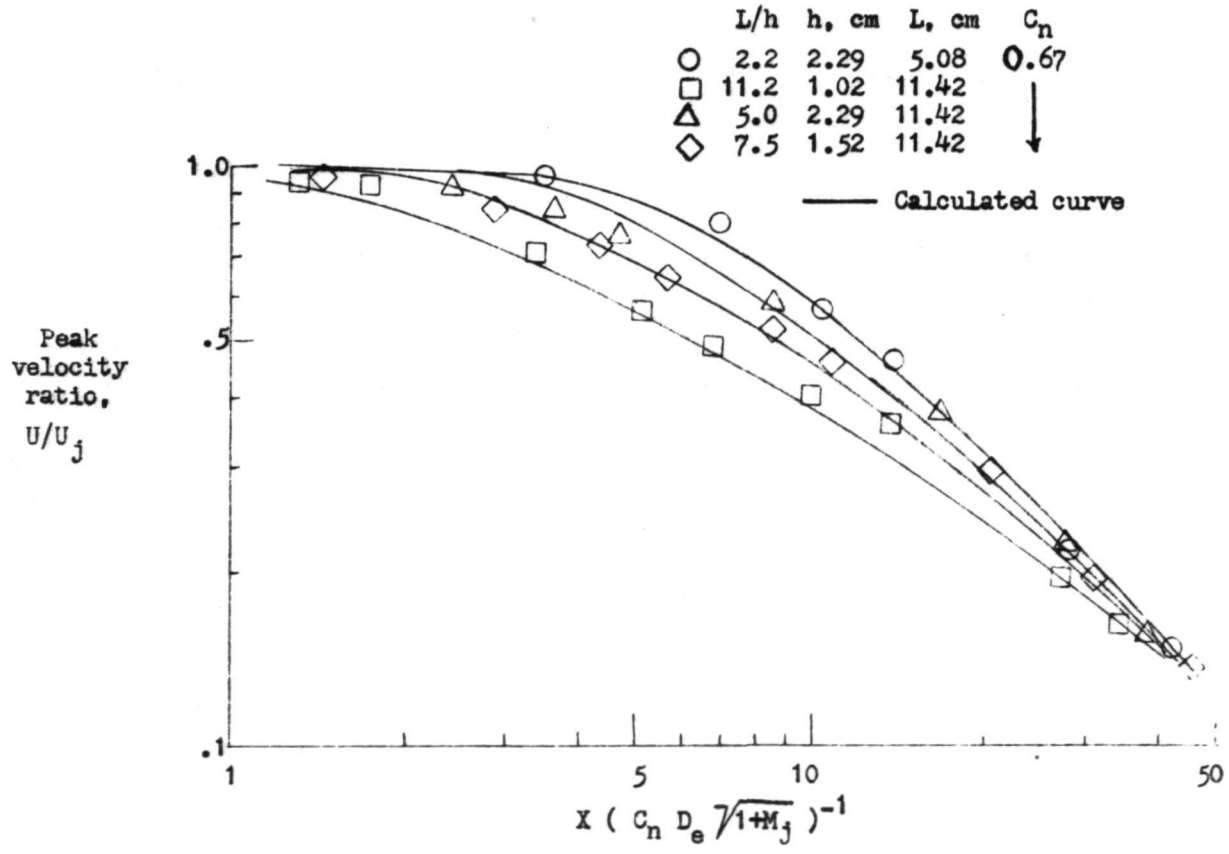

Figure 7. - Peak axial-velocity decay data for several sharp-edged, rectangular orifice-type nozzles.

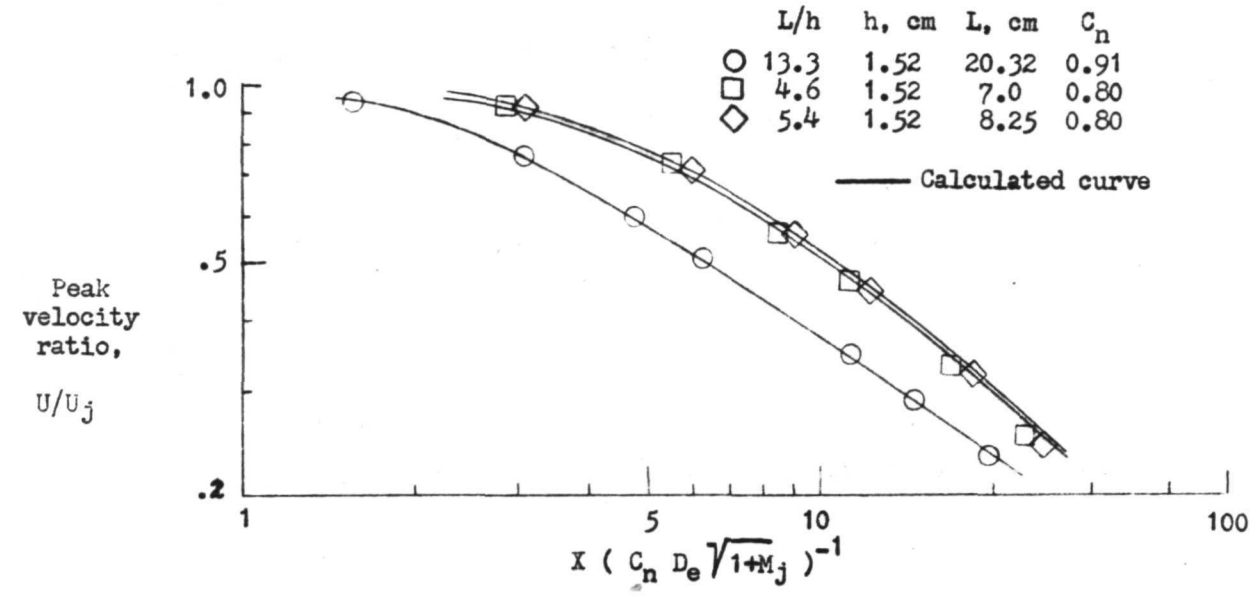

(a) Present work

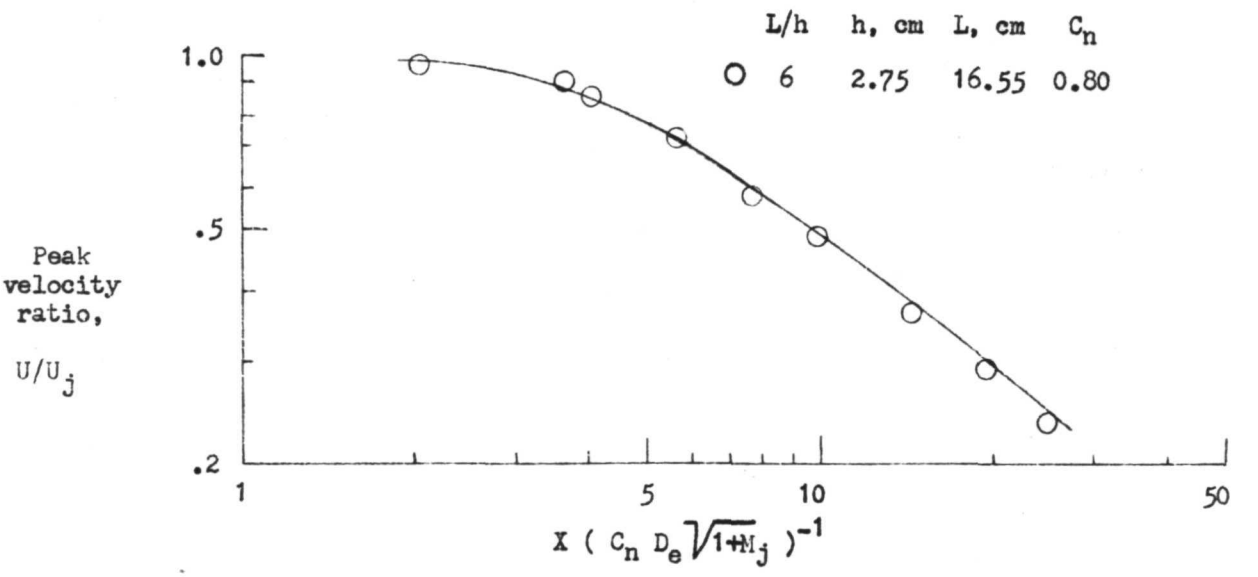

(b) References 4 and 5.

Figure 8. - Peak axial-velocity decay data for four convergent rectangular nozzles.

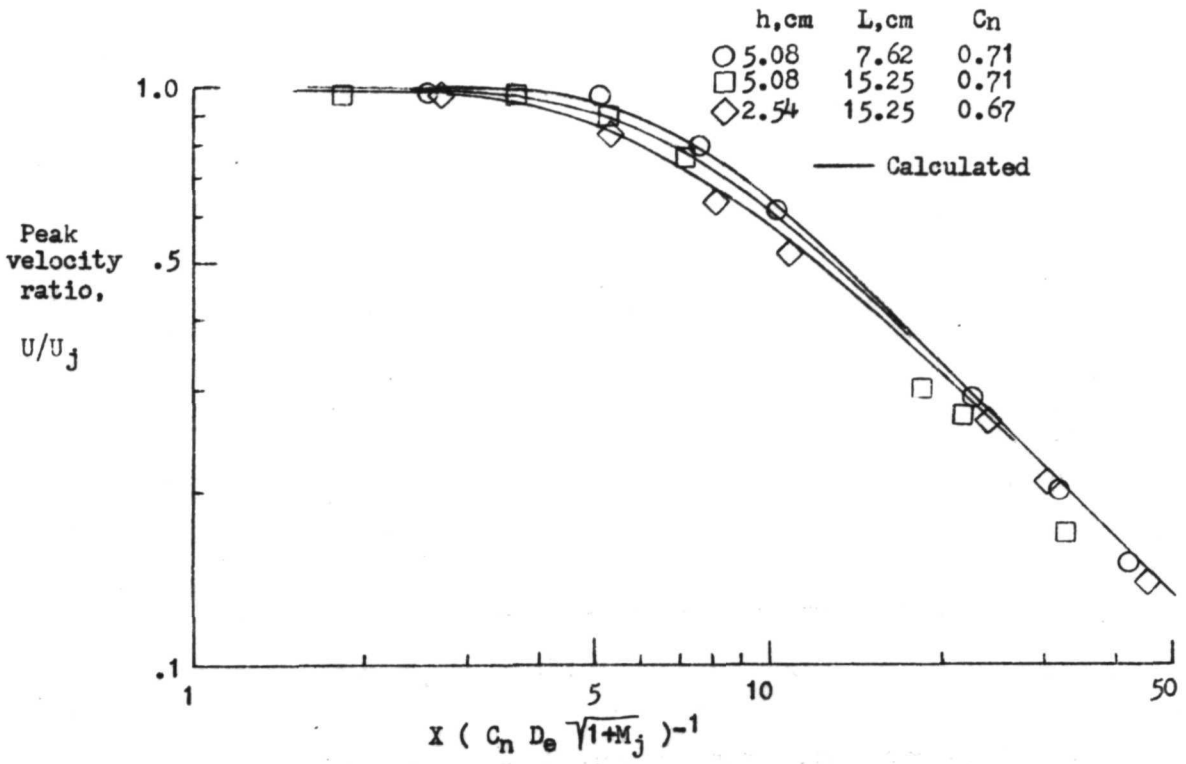

Figure 9. - Peak axial-velocity decay data for several sharp-edged triangular orifice-type nozzles. Reference 3.

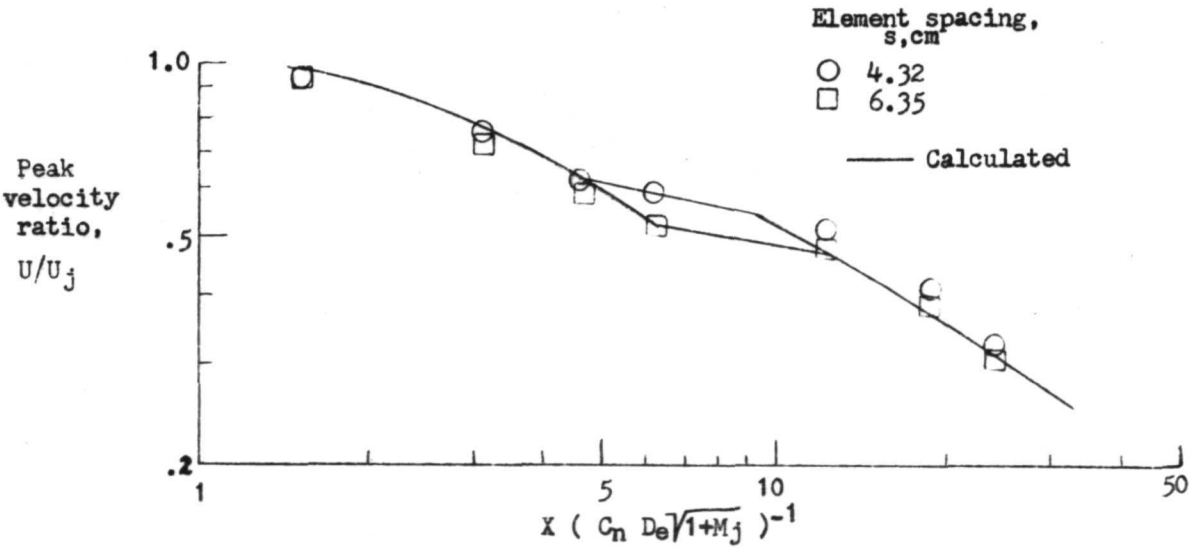

Figure 10. - Peak axial-velocity decay data for 3-slot convergent rectangular nozzle. h, 1.52 cm; L, 20.32 cm; C_n, 0.91.

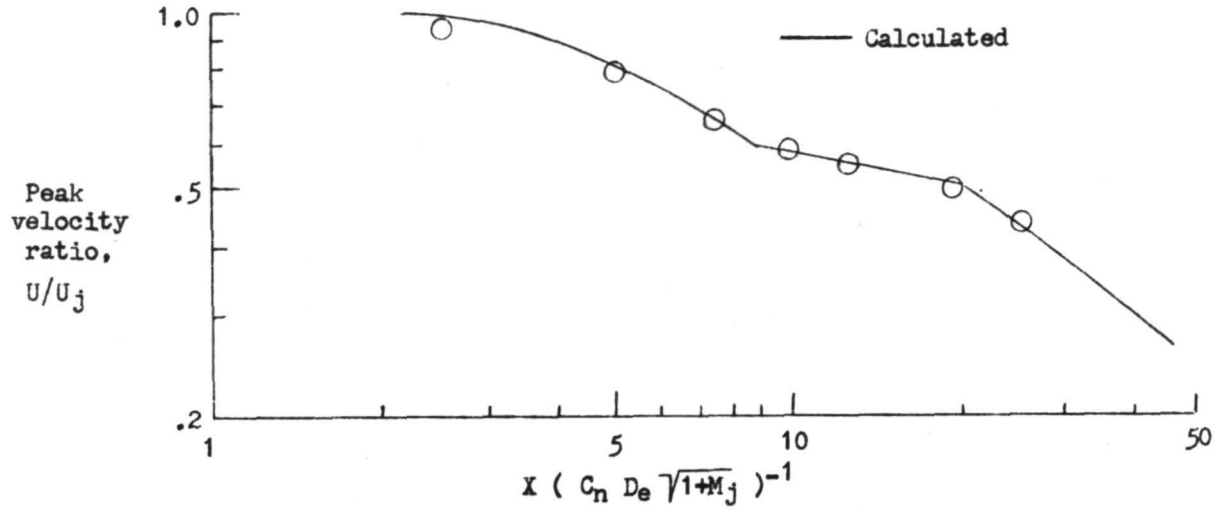

Figure 11. - Peak axial-velocity decay data for a 4-slot convergent rectangular nozzle. Reference 5; h, 1.51 cm; L, 7.55 cm; C_n, 0.55; β, 0°, s/h, 2.0.

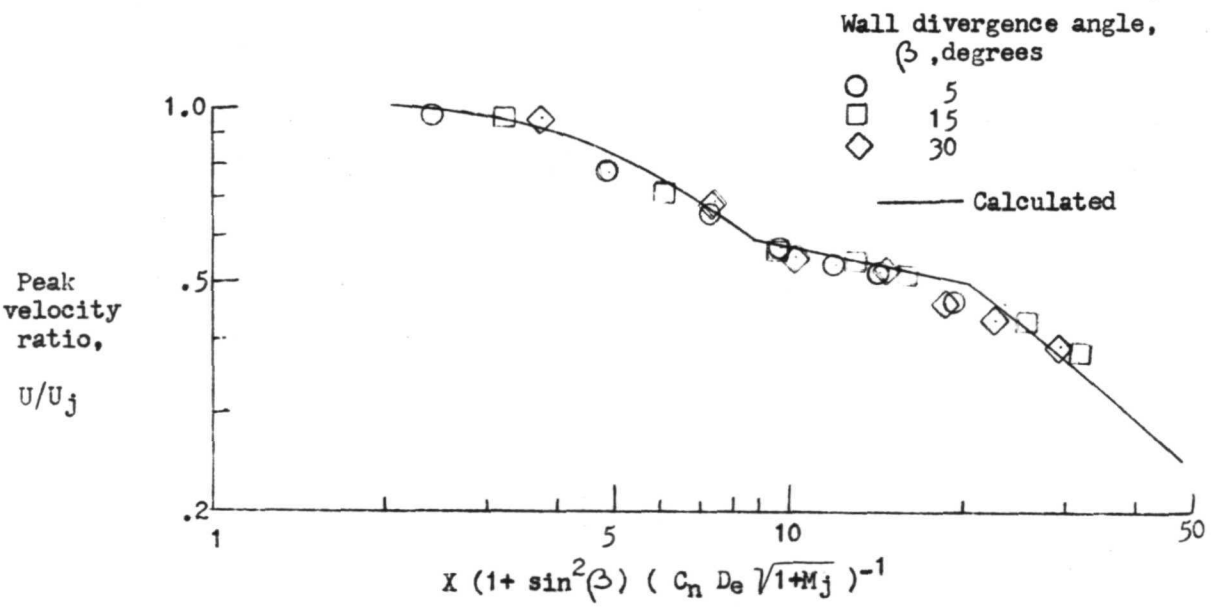

Figure 12. - Correlation of peak axial-velocity decay data for a 4-slot convergent rectangular nozzle (see fig.11) with several wall divergence angles. Reference 5; C_n, 0.55; s/h, 2.0.

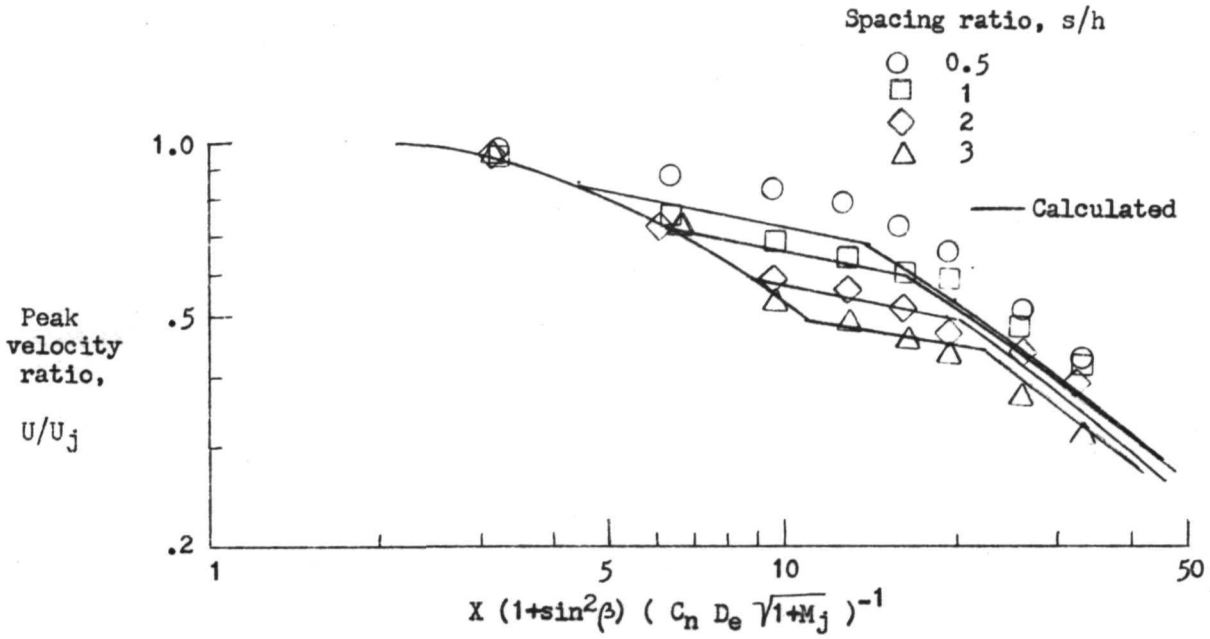

Figure 13. - Effect of element spacing ratio on peak axial-velocity ratio and decay for a 4-slot convergent rectangular nozzle (see figure 11). C_n, 0.55; β, 15°; Reference 5.

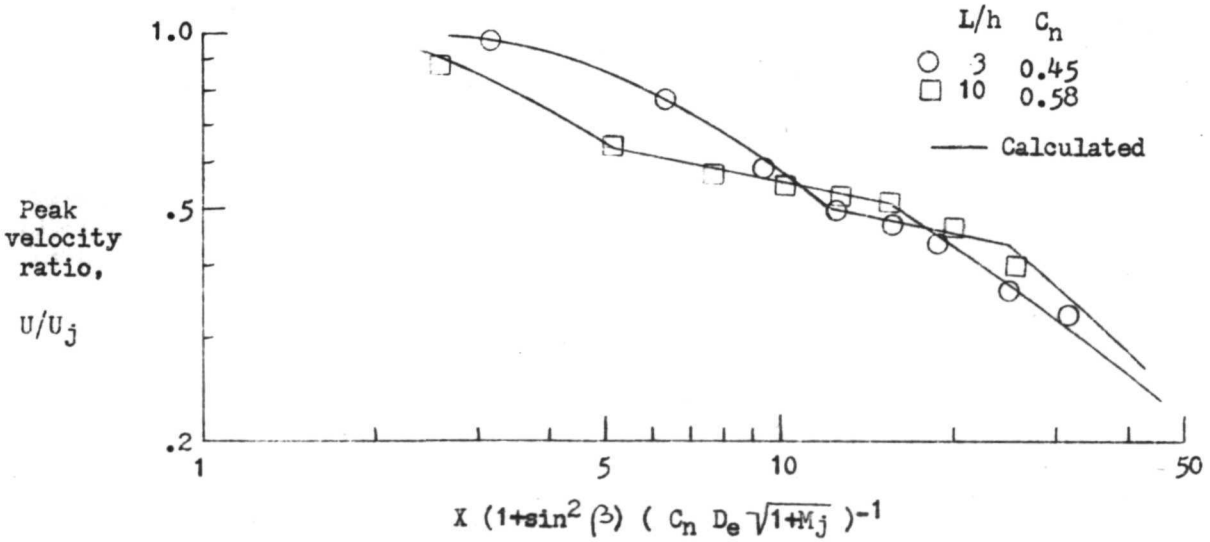

Figure 14. - Effect of aspect ratio,(L/h), on peak axial-velocity decay for a 4-slot convergent rectangular nozzle. s/h, 2.0; β, 15°; Reference 5.

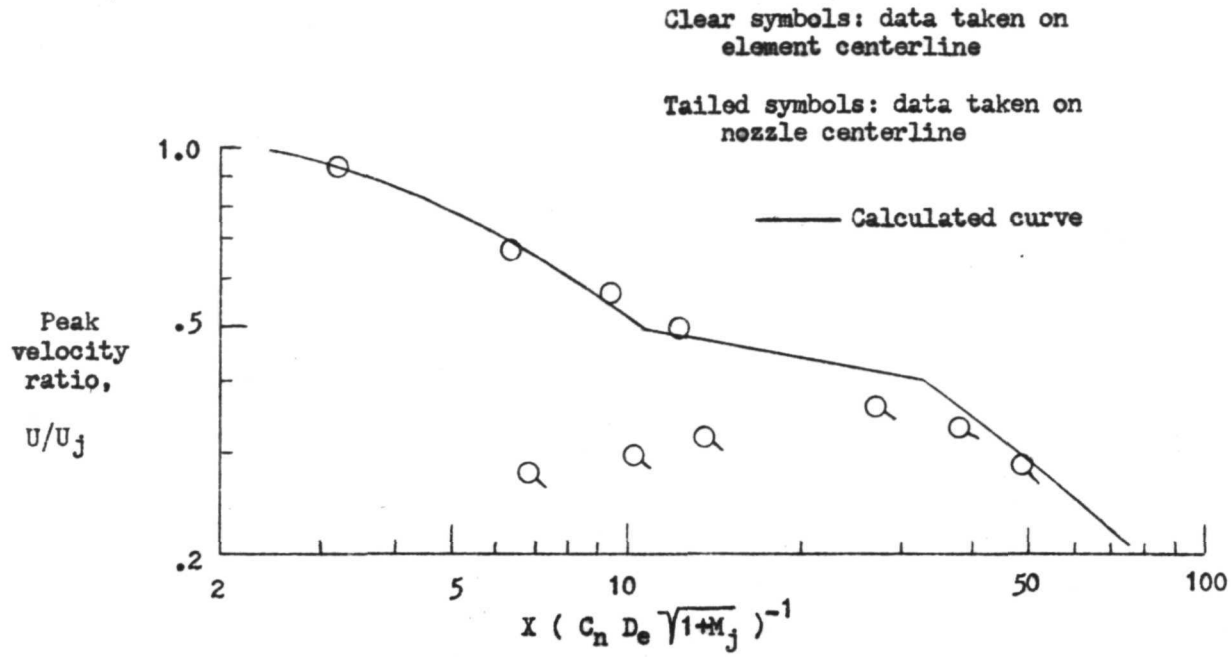

(a) L/h, 4.6; s_H, 6.35 cm; h, 1.52 cm; L, 7 cm; C_n, 0.71 .

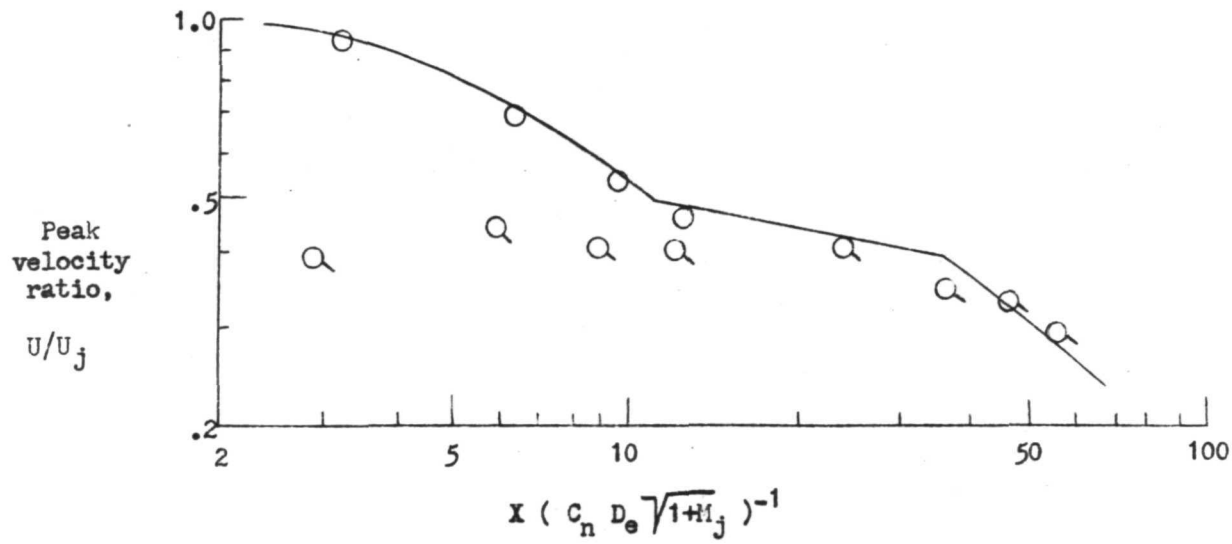

(b) L/h, 5.4; s_H, 3.81 cm; h, 1.52 cm; L, 8.25; C_n, 0.75.

Figure 15. - Peak axial-velocity decay data for 6-slot ventilated nozzles.

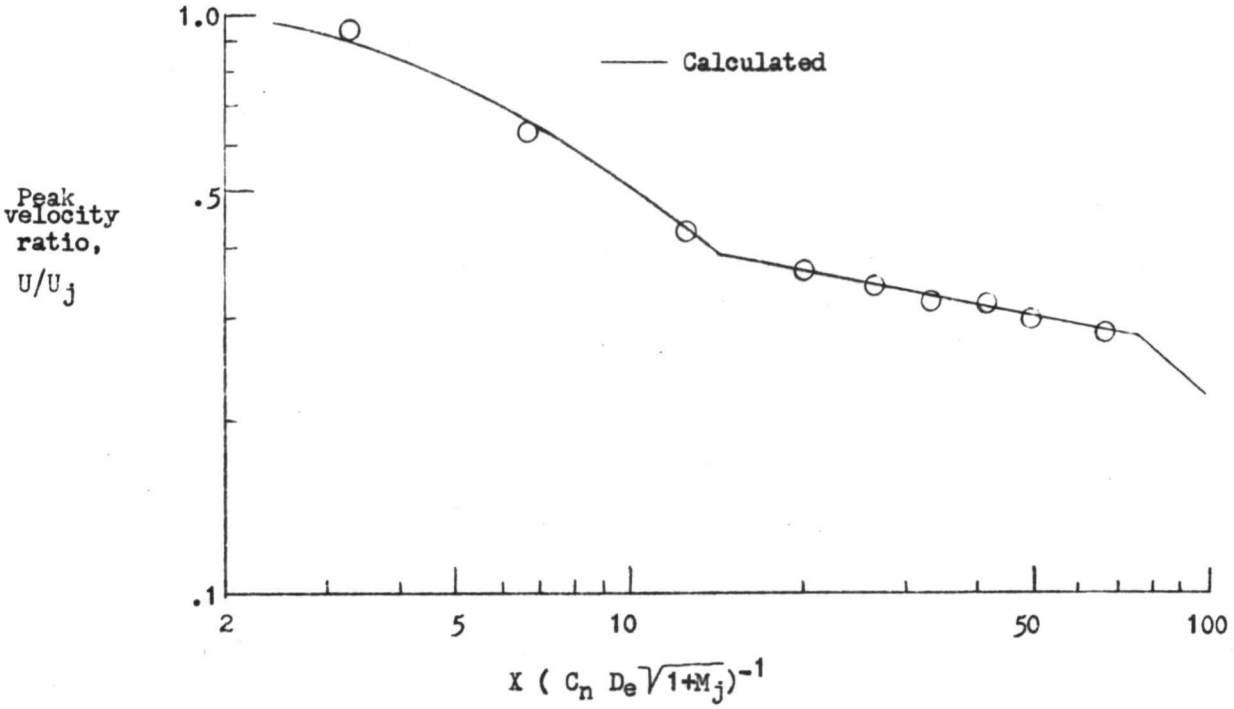

Figure 16. - Peak axial-velocity decay data for 12-lobed, triangular-element nozzle. Reference 4; nozzle pressure ratio, 1.5; C_n, 0.8; s/h, 4.0.